



A continental scale analysis reveals widespread root bimodality

Received: 3 October 2022

Accepted: 13 May 2025

Published online: 17 June 2025

Check for updates

Mingzhen Lu ^{1,2,3}, Sili Wang ⁴, Avni Malhotra ^{2,5,6},
Shersingh Joseph Tumber-Dávila ^{2,7,8}, Samantha Weintraub-Leff ⁹,
M. Luke McCormack ¹⁰, Xingchen Tony Wang ¹¹ & Robert B. Jackson ^{2,12}

An improved understanding of root vertical distribution is crucial for assessing plant-soil-atmosphere interactions and their influence on the land carbon sink. Here, we analyze a continental-scale dataset of fine roots reaching 2 meters depth, spanning from Alaskan tundra to Puerto Rican forests. Contrary to the expectation that fine root abundance decays exponentially with depth, we found root bimodality at ~20% of 44 sites, with secondary biomass peaks often below 1 m. Root bimodality was more likely in areas with low total fine root biomass and was more frequent in shrublands than grasslands. Notably, secondary peaks coincided with high soil nitrogen content at depth. Our analyses suggest that deep soil nutrients tend to be underexploited, while root bimodality offers plants a mechanism to tap into deep soil resources. Our findings add to the growing recognition that deep soil dynamics are systematically overlooked, and calls for more research attention to this deep frontier in the face of global environmental change.

Terrestrial ecosystems face a pressing challenge due to increasing atmospheric CO₂ concentration: how can land plants satisfy their increasing nutrient demand^{1–3} and consequently sustain the terrestrial carbon sink^{4–7}? A central piece to this puzzle is the ecology of plant roots. Plant roots not only are key to the uptake of growth-limiting soil resources⁸, but are also central to soil carbon input through root turnover^{9–12} and carbon loss through priming^{13,14}.

Recent studies have greatly improved our understanding of plant roots through the study of their “traits”, ranging from morphological traits such as root diameter^{15–18} to root-symbiont relationships such as mycorrhizal colonization rate^{19,20}, in part thanks to the rise of publicly available harmonized root trait data^{21–23}. However, these trait data mostly reflect micro-scale properties of individual root segments (e.g., root diameter, root nitrogen concentration). A rooting-system level understanding of how these roots are distributed throughout the soil

matrix still lags far behind (but see ref. 24), limiting our ability to scale up local, trait-based measurements to ecosystem-scale properties.

In particular, the ecology of deep fine roots (>1 m depth) is perhaps the least understood component of root ecology due to the difficulty in sampling them^{25–29}. Previous studies have reported the importance of deep fine roots in aiding plants to take up deep water³⁰, tap into deep soil nutrient reservoirs³¹ and convert photosynthetic carbon into deep soil organic matter with high efficiency³². Yet, despite the importance of deep fine roots, our decades of understanding of plant rooting systems has been mostly confined to the top 5–100 cm³³ due to the paucity of deeper fine root data^{22,34}.

The recently established National Ecological Observatory Network (NEON hereafter) uniquely addresses this data gap³⁵. First and most importantly, the NEON soil megapit data (Methods) reaches an impressive depth of 2 meters below the surface, allowing us to

¹Santa Fe Institute, Santa Fe, NM, USA. ²Department of Earth System Science, Stanford University, Stanford, CA, USA. ³Department of Environmental Studies, New York University, New York, NY, USA. ⁴Industrial Engineering and Operations Research, Columbia University, New York, USA. ⁵Department of Geography, University of Zurich, Zurich, Switzerland. ⁶Biological Sciences Division, Pacific Northwest National Laboratory, Richland, WA, USA. ⁷Harvard Forest, Harvard University, Petersham, MA, USA. ⁸Department of Environmental Studies, Dartmouth College, Hanover, NH, USA. ⁹National Ecological Observatory Network, Battelle, Boulder, CO, USA. ¹⁰Center for Tree Science, The Morton Arboretum, Lisle, IL, USA. ¹¹Department of Earth and Environmental Sciences, Boston College, Chestnut Hill, MA, USA. ¹²Woods Institute for the Environment and Precourt Institute for Energy, Stanford University, Stanford, CA, USA.

e-mail: mingzhen.lu@nyu.edu

examine fine roots to an unprecedented depth (Supplementary Fig. 2, Supplementary Table 1). Second, the NEON megapit root data are coupled with data on soil nutrients, soil physical properties, and soil moisture, making it possible to link root distributions to various abiotic factors. Third, the same standardized sampling approach is repeated across 44 sites ranging from Alaskan tundra to Puerto Rican neotropical forest³⁶, enabling us to perform continental scale analysis across a range of ecosystem types and climate zones.

Leveraging these unique strengths of the NEON dataset, in this work, we address three central questions regarding the ecology of deep roots: (1) How does the abundance of fine roots change with depth? (2) What are the factors that impact the distribution of fine roots with depth? (3) Are nutrients in deeper soils equally, under-, or over-exploited by fine roots compared with surface soil? We find widespread occurrences of fine-root bimodality across ecosystems, with nearly 20% of sites showing this previously undocumented pattern. This bimodality is linked to lower total fine-root biomass and the presence of deeper nitrogen-rich soil layers, suggesting that subsoil nutrients are systematically under-exploited by fine roots.

Results and discussion

Deep sampling reveals unexpectedly widespread root bimodality

We first examined the distribution of fine-root biomass along soil profiles up to 2 m depth. Unexpectedly, we frequently observed bimodal distributions of fine-root abundance (i.e., dry root biomass per volume), which differs from the default expectation of exponential-decay distribution^{37,38}. In Fig. 1, we show the fine-root distribution at site SCBI (Smith Conservation Biology Institute NEON) as an example of root bimodality, in contrast to the typical unimodal exponential-decay at site YELL (Yellowstone National Park NEON). The bimodal SCBI site's secondary peak of fine root biomass is found well beneath the soil surface (~1.3 m, Supplementary Table 1), and well beyond the 30 cm or rarely 1 m depth where most sampling efforts stop^{22,34}.

What's more, this surprising phenomenon of bimodal rooting distribution is widespread across the continental US, displaying no apparent patterning with regards to spatial clustering (Fig. 1c; bimodal sites in red, unimodal in blue). We estimate that 9 out of 44 (~ 20%) sites in the NEON dataset have bimodal root distributions (see Methods). It is especially noteworthy that all of these bimodal sites feature a secondary root peak deeper than 60 cm (with 33% deeper than 1 m; Supplementary Table 1), meaning these sites would not have been classified as bimodal using more common, shallower sampling depths.

As a natural phenomenon, bimodality has been widely spotted across multiple science disciplines: the bimodal body mass of African weaver ants³⁹, the bimodal mycorrhizal association in tropical rainforest¹⁹, the distribution of water vapor in Earth's atmospheric system⁴⁰, all the way to the color and shape distribution of galaxies in our cosmos⁴¹. The observation of bimodality often indicates the coexistence of two contrasting regimes/processes, of which the underlying mechanism is so far unaccounted for, raising the question of what process can give rise to the observed root bimodality.

Intuitively, if there exists a singular mechanism underlying all these bimodal root distributions (9 out of 44 NEON sites), there is a good chance we can detect the mechanism using statistical tools. In reality however, many processes can potentially cause bimodality of fine roots. For instance, the presence of a buried soil horizon rich in nutrients, surface drought coupled with presence of water supply in deeper soil, the presence of certain species that specialize in foraging for deep soil resources, and ecosystems that have documented binary niche partitioning^{42,43}, to name a few. The potential multi-cause of bimodality and the inherent heterogeneity of edaphic conditions might limit our ability to derive an universal explaining mechanism. But failure to pin down a singular universal cause would then suggest that different NEON sites might operate under very different rules and bimodality might be due to distinct site-specific mechanisms. In the next two sections, we evaluate how root bimodality is linked to a range of factors, across and within the NEON sites.

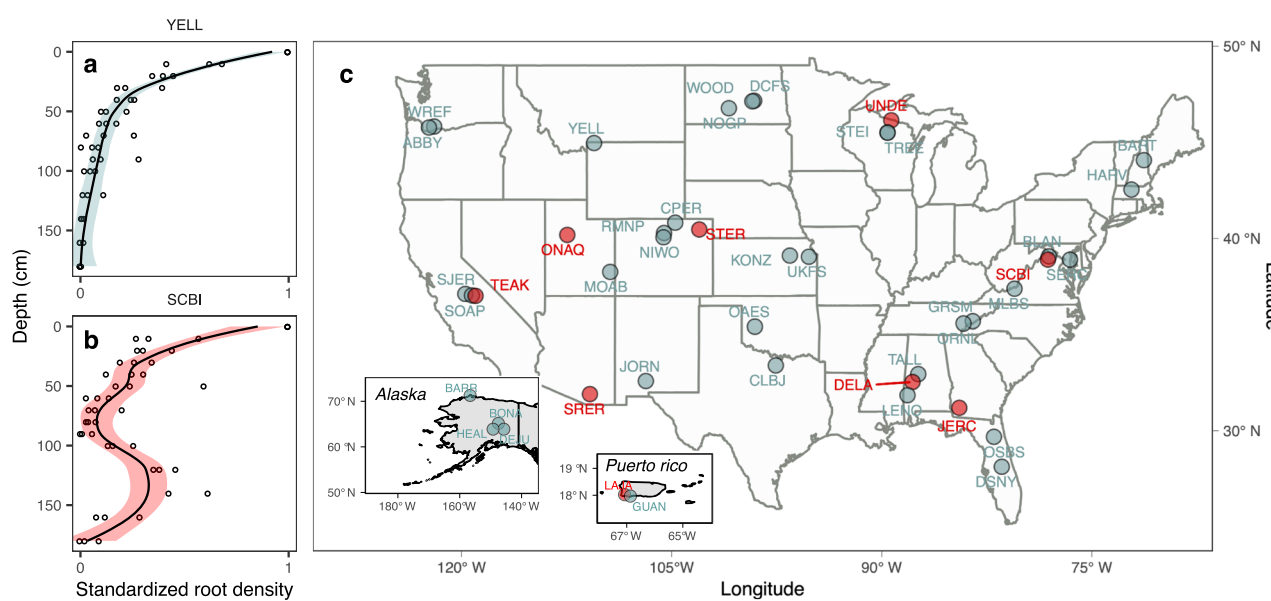


Fig. 1 | Example rooting depth profiles and the widespread bimodal rooting distribution across the NEON network. **a** An example depth profile (YELL, Yellowstone National Park NEON) of the classical exponential decay of root abundance with increasing depth. **b** An example depth profile (SCBI, Smith Conservation Biology Institute NEON) of a bimodal rooting distribution shows a secondary peak of root biomass far beneath the soil surface. Note that the root abundance is standardized based on the maximum abundance to facilitate visualization and

cross-site comparison. Error bands represent the 95% confidence intervals around LOESS fits (solid black), with red fill denoting bimodal distribution and blue denoting the unimodal exponential decay. **c** The spatial distribution of rooting profiles across 44 NEON sites (R package “maps v3.4.2”). Detailed site descriptions can be found in Supplementary Table 1 along with all 44 rooting profiles (Fig. S2). Source data are provided as a Source Data file.

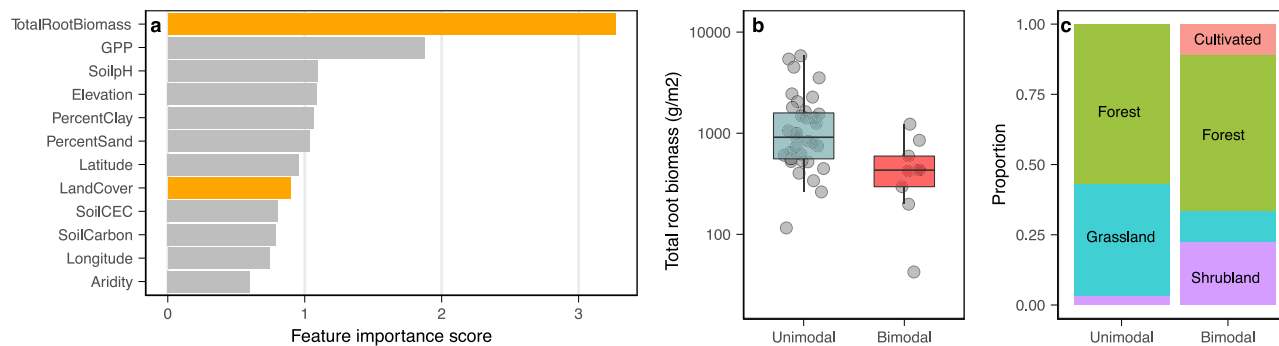


Fig. 2 | Root bimodality predicted by site-level factors. **a** Feature importance ranking from a random forest classification model (Methods) identify total fine root biomass (g/m^2) as the most important factor in predicting the modality of a site. Of these 12 factors (see Methods, site-level factors), land cover is the only categorical variable, the rest are continuous. The features in the orange bars are highlighted in **(b, c)**. **b** Unimodal sites ($n = 35$, 990 g/m^2) have nearly 3 times more root biomass than that of bimodal sites ($n = 9$, 368 g/m^2 ; two-sided Student's t-test, $p = 0.004$). Note that y axis is on logarithmic scale. **c** Site modality (bimodal vs. unimodal) are

not independently distributed across vegetation types (forest in green, grassland in blue, shrubland in purple, cultivated in red). Bimodal sites are more frequently associated with shrubland but less with grassland (two-sided chi-square test, $p = 0.019$, $\chi^2 = 9.6$). In each box plot, the lower and upper bounds of the whiskers denote minima and maxima, the center line denotes the median, and the lower and upper bounds of the boxes represent the 25% and 75% quantiles, respectively. Source data are provided as a Source Data file.

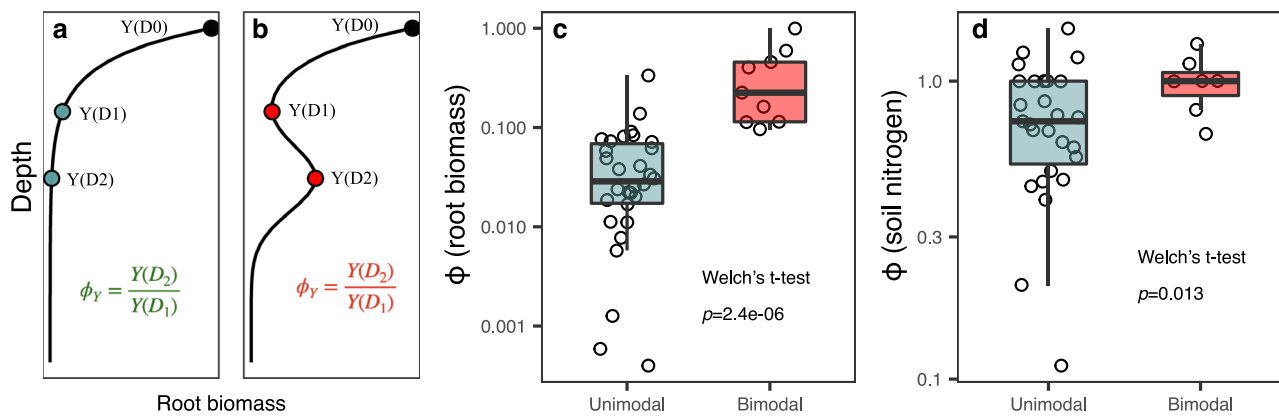


Fig. 3 | Root bimodality explained by within-site depth-level factors. **a, b** Illustration of a unimodal distribution **(a)** and a bimodal distribution **(b)** of property Y (root biomass in this case). Three depths derived from bimodal distribution are highlighted with filled dots: primary mode depth (D_0), antimode depth (D_1), and secondary mode depth (D_2) (Methods). Using a given property value (Y) at depth D_1 and D_2 , we can calculate ϕ as the ratio of $Y(D_2)$ and $Y(D_1)$. **c** Comparison of ϕ (root biomass) across unimodal ($n = 35$) and bimodal ($n = 9$) sites

(two-sided Welch's t-test, $p = 2.4 \times 10^{-6}$). **d** Comparison of ϕ (soil nitrogen concentration) across unimodal ($n = 27$) and bimodal ($n = 7$) sites (two-sided Welch's t-test, $p = 0.013$). Note that ϕ is unitless. In each box plot, the lower and upper bounds of the whiskers denote minima and maxima, the center line denotes the median, and the lower and upper bounds of the boxes represent the 25% and 75% quantiles, respectively. Source data are provided as a Source Data file.

Bimodality linked to site-level factors

We first analyzed whether the presence of root bimodality is linked to site-level features across all NEON sites. We built a classification model that takes into account 12 site-level features (Methods, Fig. 2a, S3) to examine the predictive power of each feature for bimodality. We chose a random forest algorithm for our classification model because (1) it is robust to the presence of outliers and nonlinear relationships and (2) it has a built-in validation mechanism that is particularly valuable for our small sample size (44 NEON sites). The resulting best performing classification model achieved an overall accuracy of 64% (correctly predicting the modality of 28 out of 44 sites), with a 66.7% accuracy for predicting bimodal and 63% accuracy for predicting unimodal sites. The importance ranking of features (Fig. 2a) from this classification model identifies total fine root biomass (g/m^2 ; per square meter surface to maximal pit depth) as the most important predictor of bimodality, followed by gross primary production (GPP), and a range of other features.

Out of the 12 factors analyzed, we selected two (one continuous and one categorical) to visualize differences among sites associated with bimodality in more detail (see Supplementary Fig. 4 for the other 10 factors). Figure 2b reveals that unimodal sites have nearly 3 times total fine root biomass compared to that of bimodal sites ($990 \text{ vs. } 368 \text{ g/m}^2$). This pattern is rather unexpected yet significant despite the small sample size ($p = 0.004$, student's t-test). We also show that site vegetation cover is associated with site modality (Fig. 3c; $p = 0.019$, $\chi^2 = 9.6$; Methods). While the majority of bimodal sites are forested, bimodality is more frequently associated with shrublands than with grasslands. We also explored whether classifying sites based on growth forms (woody vs. herbaceous) would help explain the occurrence of bimodality. Due to the small sample size ($N = 44$), we did not find significant evidence to support an association between bimodality and growth form ($p = 0.43$, $\chi^2 = 0.98$). However, that doesn't rule out the possibility of growth-form playing an important role. Our analysis thus calls for more extensive sampling efforts.

When we removed total fine root biomass from our predictive model, the resulting model had little predictive power, suggesting that no environmental factor is a universal cause for root bimodality across all sites. This result, however, does not rule out the possibility that these factors might be important at each individual site. In fact, the finding that bimodality is strongly linked to root biomass suggests that factors that can induce low root biomass might be important for inducing root bimodality (e.g., high aridity, low GPP, low soil pH, inherent species differences), but the specific cause of low root biomass at each site can be different.

Water- or nitrogen- driven: a depth-level analysis of bimodality

We next zoom into within-site factors along the soil depth profile (*i.e.*, depth-level) to examine whether soil nutrient concentrations and/or soil moisture may play a role in the emergence of root bimodality. To quantify the degree of bimodality in root biomass and its associated predictors, we devised a signature metric ϕ defined as the ratio of $Y(D_2)$ and $Y(D_1)$ where D_2 is the depth of secondary root biomass mode, D_1 the antimode (D_0 for primary mode, see Fig. 3b), and Y denotes properties such as root biomass density, soil moisture, soil nutrient content, etc. (Fig. 3a, b).

By the definition of bimodality, when we calculate ϕ for root biomass across 44 sites, bimodal sites have significantly higher ϕ value than unimodal sites (Fig. 3c; $p = 2.4e-6$, Student's t-test). When we extend this analysis to a range of soil conditions (nutrient content, soil texture, soil moisture, etc.), our results only identify an analogous pattern in soil nitrogen concentration: bimodal sites contain significantly more nitrogen at depth D_2 compared with the default expectation (Fig. 3d).

Two alternative mechanisms might explain the presence of a nitrogen rich layer that coincides with the secondary peak of root biomass: the “nitrogen-driven hypothesis” and the “water-driven hypothesis”.

For the “nitrogen-driven hypothesis”, we speculate that the presence of nitrogen in the soil can induce fine root growth. It is not uncommon that nutrient concentrations can feature a secondary peak in deep soil due to a number of factors, such as weathering of primary rock (albeit low concentrations^{44,45}), accumulation of nutrients beyond the typical root uptake zone⁴⁶, and the presence of buried soil horizons rich in nutrients⁴⁷. In turn, these deep nutrient anomalies can trigger the growth of fine roots which are responsible for foraging for limiting nutrients. This ability of roots to respond to nutrient cues has been extensively demonstrated by physiology literature looking at root production in response to localized chemical cues⁴⁸, or in response to heterogenous nutrient patches in the soil matrix⁴⁹.

However, the presence of deep nitrogen-rich layers could also be the result –instead of the cause– of the abundant fine roots, which might be produced to forage for other limiting resources such as water (“water-driven hypothesis”) or phosphorus. It is well known that the presence and turnover of fine roots can build up soil organic matter and consequently soil nitrogen^{9,50}. It is thus possible that the nitrogen layer can be caused by the decay of water-seeking or phosphorus-seeking fine roots.

Potentially due to the limited depth-resolution of soil moisture sensors (Methods), we didn't find definitive evidence that supports the presence of a soil moisture peak coinciding with the presence of a secondary root peak. Specifically, when we analyzed long-term dynamics of soil moisture ($\phi_{\text{soil moisture}}$) between unimodal vs. bimodal sites, we found no meaningful difference (Supplementary Fig. 5; Methods). In evaluating whether surface drought might induce bimodality, an in-depth look at surface soil moisture (at D_0) did not render a consistent difference between bimodal vs. unimodal sites (Supplementary Fig. 6). However, in natural ecosystems, fine roots are very plastic and responsive to localized and temporally brief supply of water⁵¹. It is thus entirely possible that the lack of support for the

“water-driven hypothesis” was simply due to low spatial resolution of soil moisture data.

The “nitrogen-driven hypothesis” and the “water-driven hypothesis” do not have to be mutually exclusive. After all, the process of nitrogen mineralization – microbial release of available nitrogen from soil organic matter–is often limited by water availability⁵². Moreover, it is very likely that different mechanisms (water, or different types of nutrients) might be causing bimodality at different sites. For instance, we didn't find statistical support for phosphorus driving root bimodality, yet we cannot rule out the possibility of foraging for phosphorus being the cause of root bimodality at certain NEON sites, especially because only total rather than available phosphorus was measured at the 44 sites. Future studies with higher spatial resolution, especially controlled experiments, might help us address these unresolved questions.

Implications of root bimodality for subsoil nutrients and carbon

To evaluate the potential impact of root bimodality on plant resource uptake, we next analyzed the spatial distribution of soil nutrients in relation to the vertical distribution of roots. We choose to use root biomass as a surrogate for root uptake as some biomass proliferation represents a direct plant investment for resource acquisition. In natural settings, however, the realized uptake rate often depends on nutrient availability in the soil solution⁵³. But the use of root biomass provides a good estimate of resource uptake potential, as one would expect strong correlation between root biomass and realized nutrient uptake when averaged over time and space. Alternative metrics for root uptake also include root surface area and root length (not available in our dataset); both correlate with root biomass.

When expressed relative to the abundance of fine root biomass (see Methods), relative soil nutrients appear to increase in abundance with increasing depth. For example, the relative phosphorus (P) abundance from site “YELL” (Yellowstone National Park NEON) increases with depth (Fig. 4a; $r^2 = 0.85$), indicating that subsoil phosphorus is becoming relatively more abundant from the perspective of the roots.

We can expand the example analysis in Fig. 4a to all 44 NEON sites and across four major soil nutrients: nitrogen (N), phosphorus (P), potassium (K), and calcium (Ca) (Supplementary Figs. 7–10). We can summarize the exponents across all sites for each individual nutrient, with each datapoint in Supplementary Fig. 11 corresponding to the slope value of a given NEON site (for example, 0.013 in Fig. 4a for P at YELL). Despite considerable variation across sites, our results clearly identify a general trend across the unimodal sites similar to what is shown in Fig. 4a: root abundance decays relatively faster than nutrients with increasing depth, leading to increasing relative nutrient abundance (*i.e.*, positive exponent).

However, the presence of bimodal root distribution seems to disrupt the aforementioned general trend: the subsoil relative nutrient concentration in bimodal site (red area in Fig. 4b, site SCBI) is dramatically lower compared to the expectation set up by the unimodal site (red area in Fig. 4a, site YELL). And consequently, the goodness of regression fit is much poorer for bimodal sites across all nutrient types (Supplementary Fig. 12).

Our finding that soil nutrients become relatively more abundant relative to root biomass with increasing soil depth suggests that subsoil resources might be systematically under-exploited by plant roots (Fig. 4a, Supplementary Fig. 11). This finding is puzzling given how frequently nitrogen⁵⁴, phosphorus⁵⁵, potassium⁵⁶, and calcium^{57,58} can limit the productivity of terrestrial ecosystems, pointing to some fundamental constraints that limit plant roots to exploit subsoil. For example, many studies have argued that plants preferentially use resources from shallower depths due to: 1) the high carbon cost associated with growing deeper root systems, 2) morphologically-induced hydraulic limitations, 3) the evaporative demand of acquiring

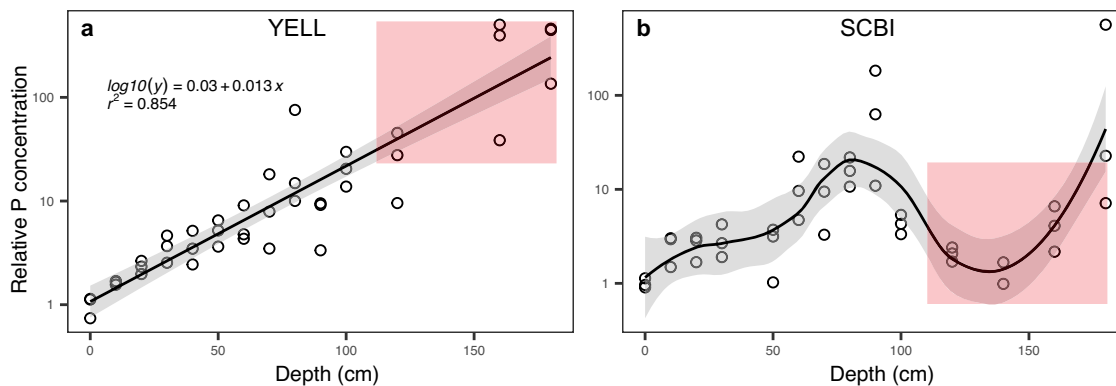


Fig. 4 | Relative nutrient concentration changes with soil depth in an unimodal and a bimodal site. **a** We calculated relative nutrient concentration by dividing absolute nutrient concentration by the root biomass. For ease of comparison across sites, we rescaled relative root biomass by dividing relative biomass using topsoil (Depth=0 cm) relative nutrient concentration is 1 (i.e., dimensionless, see Methods). Using YELL (Yellowstone National Park NEON) as an example, both soil P content and root abundance decrease exponentially with increasing soil depth, but root abundance decays at a faster pace with depth. The resulting relative P concentration (black circle) increases exponentially with increasing soil depth (exponent = 0.013). This pattern suggests that as soil

depth increases, nutrients become comparatively more abundant or under-exploited in the subsoil (red area 1). Note that the Y axis is in logarithmic scale and the goodness of fit (r^2) applies to the corresponding linear regression ($\log_{10}(y)$ instead of y). Gray ribbon represents the 95% confidence intervals around linear regression. **b** Using SCBI (Smith Conservation Biology Institute NEON) as an example, the presence of bimodal root distribution generates a region of low relative nutrient concentration in the subsoil (red area 2). Given the presence of root bimodality rendering a linear regression (on log scale) unfit for this analysis, we used loess fit (span=0.5) to capture the nonlinearity. Gray ribbon represents the 95% confidence interval for loess fit. Source data are provided as a Source Data file.

resources from deeper depths, and 4) declining oxygen concentrations impeding root growth at depth^{46,59–63}.

However, the discovery of bimodal root distribution across a range of sites suggests otherwise (Fig. 1, Fig. 4b). In fact, the presence of root bimodality indicates that root depth distribution can be flexible and opportunistic: given the right condition, plants can send abundant roots to deep soil. Numerous previous studies corroborate this argument. For example, Iversen et al. (2010) reviewed the change of root distribution in response to elevated CO₂ treatment⁶⁴, and discovered that roots can “dig deeper” with increased carbon supply (and consequently higher nutrient demand). Dry sites or sites with high seasonality in precipitation have also shown evidence of flexible bimodal distributions wherein the depth of water uptake becomes deep in the dry season and shallow in the wet season^{65–68}.

The carbon consequence of enhanced root growth in deep soil can be far-reaching¹⁴. On the one hand, we would expect enhanced input of new carbon due to root turnover. Deep soil carbon relies much more on root carbon input than aboveground litter input^{9,11,69}. And once root carbon is deposited, the carbon decomposition rate can be 60% slower compared with the rate derived from the surface soil^{11,70}, in part due to the combined effect of lower microbial community density and increased mineral protection^{71–73}. Alternatively, we might also expect enhanced decomposition of old carbon induced by root production at deeper depths: physical disturbance of carbon-mineral complex⁷⁴, impacts on the soil food web⁷⁵, and enhanced microbial activities through priming effects^{76–78} can lead to potential destabilization of subsoil.

The implications of our finding can be profound especially against the backdrop of rapid global change. An extensive literature examines the role of increasing CO₂ in driving an increasing degree of plant/ecosystem scale nutrient limitation^{2,3,79}: plants are getting increased supply of carbon but increasingly less nutrients as more and more nutrients are locked up in plant biomass. The resulting progressive nutrient limitation has fueled the fear of a saturating land carbon sink⁴ due to the inability of the ecosystem to fix additional carbon^{3,5,7}. Our analyses thus suggest plants can potentially invest an increasing amount of their photosynthates to tap into the previously under-exploited soil nutrient pool as the plant cost-benefit equation is being shifted by global warming and rising CO₂.

Taken together, these findings emphasize the need for an improved understanding of the spatial distribution of plant roots, which is critical for understanding the nutritional life of land plants, and may help to predict the future trajectory of the land carbon sink. We report a surprisingly widespread occurrence of root bimodality across a broad range of ecosystems. This new understanding of the vertical distribution of plant roots could help us to better scale up point measurements to the entire soil profile, a knowledge gap especially relevant to the study of ecosystem nutrient cycles and the land carbon sink. In addition, our observation can inform the development of the next-generation mechanistic vegetation models, which for decades have relied on relatively simplistic representation of roots (if any). But perhaps more broadly, our findings add to the growing recognition that the field of soil ecology and ecosystem ecology might have systematically overlooked dynamics and phenomena taking place in the deep soil; our results call for more research attention to this deep frontier in the face of rapid environmental change.

Methods

NEON mega-pit and associated soil dataset

At each terrestrial field site, NEON collected soil at a single, temporary soil pit (i.e., the megapit). The pit was selected to be in the locally dominant soil type and within a few hundred meters of the instrumented NEON tower and soil sensors. At non-permafrost sites the soil pit was 2 m deep or extended to bedrock or other restrictive feature, whichever was shallower. Since soil sensors were placed up to 3 m deep to monitor changes in permafrost at some Alaskan sites, these soil pits were up to 3 m deep (yet note that root sampling only extends to 2 m regardless of pit depth, Supplementary Fig. 2). For each soil pit, 5 classes of measurements and samples were collected: (1) Soil profile description, (2) Photos showing entire soil profile, as well as close-ups of each horizon, (3) Terrestrial-Instrument-System (TIS) soil archive and biogeochemistry samples collection from each horizon, (4) Bulk density sample collection from each horizon, (5) Intact soil block sample collection (≤ 6 per soil pit). The resulting soil physical and chemical properties from these samples (DP1.00096.001), includes data on the soil taxonomy, horizon names, horizon depths, soil bulk density, coarse fragment content, texture (sand, silt, and clay content), pH, electrical conductivity, and total content of a range of chemical elements in the

<2 mm soil fraction for each soil horizon. More detailed methods can be accessed from the official user guide and protocols (<https://data.neonscience.org/data-products/DP1.00096.001>).

NEON mega-pit root dataset

The megapit described above is sampled once during construction and represents a point in time. Each pit has three vertically oriented sampling profiles up to 2 meters. From the surface to 1 m, a sample of soil is removed for each 10 cm depth increment. From 1 m to 2 m depth, each profile is divided into 20 cm depth increments. Roots are then sorted into two root statuses (alive or dead) and two size classes (coarse roots and fine roots diameter). Root biomass, carbon and nitrogen content, and 13C and 15N ratios of roots sampled were analyzed. This root data was available for the majority but not all of the terrestrial NEON sites (44/47). More detailed methods can be accessed from the official user guide and protocols (<https://data.neonscience.org/data-products/DP1.10066.001>).

Throughout our analyses, we have focused on the most metabolically active component of the rooting system, the fine roots, due to their central role in water and nutrient uptake¹⁵, their fast turnover and thus central role in soil carbon dynamics^{50,80,81}. However, we do need to mention that the NEON terrestrial sites (mega-pit project in particular) used two operational definitions of fine roots: <2 mm and <4 mm. This discrepancy was caused by an accident in how different NEON technicians were using the tools to classify root diameters in the early days of the observatory. According to Supplementary Table 1, there are 30 sites that define fine roots as <2 mm while the other 14 sites use <4 mm as the cutoff. To address this issue, we conducted two side analyses that suggest that our main findings are not sensitive to the discrepancy of fine root definition. Our side analyses are as follows:

First, we analyzed literature data on the correlation between 2 mm and 4 mm root classes. Our analysis (Supplementary Note 1) reveals that biomass calculations based on different cutoffs are in fact highly correlated ($R^2 > 0.99$) such that root biomass based on 2 mm definition (B_{2mm}) can be linearly rescaled to root biomass based on 4 mm definition (B_{4mm}), or vice versa. On average, for each 1 gram of fine root observed using the <2 mm standard, one would observe ~1.3 gram of fine roots if they were to use the <4 mm standard (Supplementary Note 1). And given our main results are based on rescaled relative root biomass, the arbitrary choice of size cutoff should have little to no effect on the results. In fact, our analyses (Supplementary Note S1) suggest the possibility that findings of bimodality in fine roots (<2 mm or <4 mm cutoff) might be extended to other root classes that are harder to sample given their high degree of correlation. Second, we found that our main findings remain unaltered even if we limit our analysis to only include sites with the <2 mm standard (detailed in Supplementary Note 1, Supplementary Fig. 1).

Harmonization of depth-based root data and horizon-based soil properties

The mega-pit root biomass dataset included measurements of root biomass and associated root chemical properties at specific depth increments across various sites (1 data point per 10 cm of soil depth for the first meter and per 20 cm in the second meter of soil, in total 15 data points). However, characterization of soil horizons differ across sites. The horizon-based soil property database is about half the spatial resolution of the root biomass database. For example, the site YELL (Yellowstone National Park NEON) has a total of 8 horizons characterized (i.e., 8 data points): A (center depth 2 cm), Bt1 (16.5 cm), Bw (37 cm), Bt2 (56 cm), Btk1 (82.5 cm), Btk2 (112 cm), Btk3 (143.5 cm), Btk4 (180.5 cm), compared to the 15 root samples. In order to more robustly compare these two datasets, we “standardized” the horizon-based soil property database to a depth-based format⁸². For instance, for a given site, if the depth interval [20-30 cm] falls completely within a single horizon (for example B horizon), then we simply populate the

depth interval [20-30 cm] with soil property data from that horizon. However, if the depth interval [20-30 cm] contains a mixture of horizons (for example, 3 cm of A, 5 cm of B, 2 cm of C), we will populate that depth interval with depth-weighted average soil properties based on the specific horizon composition.

Soil moisture sensor data

We downloaded soil moisture time series from all sites with data ranging between 2018-Sep and 2021-Aug (3 year span). Soil sensor measures soil water content/ion content across a 10 cm vertical measurement zone (5 cm above and below). Sensor depth represents the center of the measurement zone, at 6 cm, 16 cm, 26 cm, 56 cm, 86 cm, 116 cm, 146 cm, 176 cm (exact depth varies across sites, exact depths can be found in our data deposit). To ensure data coverage, multiple soil moisture sensors were installed at each depth across different profiles within each site. Two temporal resolutions were provided from the soil moisture data product: 1 min resolution vs. 30 min. Given plant rooting systems are unlikely to be sensitive to 1 min-level soil moisture variation, we used soil moisture sensor data that was averaged at 30 mins (DP1.00094.001)⁸³.

Determining site modality

We first selected live fine roots from all profiles across all sites (3 profiles per site) and merged profile level data into a site level mean root biomass density (biomass per volume of soil, hereafter “root biomass”) at each depth. We then translated biomass data (double precision) into frequency of counts (integer) in order to process the modality of biomass depth distribution. Using R package “multimode”, we can derive the number, magnitude, and location of mode/modes in a distribution^{84,85}. Given the root sampling depth is not continuous according to NEON sampling procedure, we used a bandwidth of 15 cm for kernel density estimation such that the algorithm would not pick up each sampling depth as a distinct mode. We also defined a threshold for classifying bimodal distribution: the secondary peak has to be equal or larger to 10% of the magnitude of the primary peak. Increasing this cutoff value will select for sites with more prominent secondary peaks but leaves few sites qualifying. In theory, our approach allows for detection of more than 2 modes, but in practice, a maximum of 2 modes was detected (especially after applying the threshold for mode magnitude). For bimodal distribution, depth locations of each mode and antimode are recorded as (D_0, D_1, D_2) for primary mode, antimode, secondary mode respectively.

Site-level factors

We downloaded the NEON field site information table from the official NEON website (<https://www.neonscience.org/field-sites/explore-field-sites>). From this information table, we extracted the following site-level factors for our classification model (detailed in Statistics): (1) ecosystem type, (2) ecoregion, (3) land cover type, (4) elevation, (5) root biomass per profile, (6) mean annual temperature (MAT_C), (7) mean annual precipitation (MAP_mm). We further expanded the site-level climatic features by adding (8) annual temperature range (TempRange), (9) dry season precipitation (PrecipDry), and (10) precipitation seasonality (PrecipSeas) from WorldClim (<http://worldclim.org/version2>⁸⁶); (11) aridity index and (12) potential evapotranspiration (PET) from the Global-Aridity/PET geospatial database⁸⁷. To complement the climatic factors, we compiled a range of site-level edaphic features: (13) sand percentage (PercSand), (14) clay percentage (PercClay), (15) soil taxonomy (SoilTaxo), (16) soil acidity (SoilpH), (17) average cation exchange capacity (SoilCEC), (18) soil carbon content (SoilC) from the Soil Grids (<https://soilgrids.org>), and (19) soil organic carbon of the top 30 cm (SOC30cm) from the Global Soil Organic Carbon map (GSOCmap1.5, FAO). To approximate the site-level productivity, we used site-level gross primary production to derive (20) the long-term average GPP (GPP, 2000-2016)⁸⁸. Our random-forest

classification model (Statistics section) allowed us to evaluate the feature importance score (Fig. 2) of each site-level factors and their combined predictive power. We sequentially dropped the factors with the smallest importance score until the combined predictive power was maximized. The resulting 12 factors were visualized in Fig. 2 (2 factors) and Supplementary Fig. 4 (the remaining 10 factors).

Calculating ϕ

We devised a profile-level metric ϕ that describes the ratio of property $Y(D_2)$ and $Y(D_1)$ where D_2 identify the depth of secondary root biomass mode, D_1 the antimode (D_0 for primary mode), and Y denote properties such as root biomass density, soil nutrient content, soil moisture, etc (Fig. 3A, B). For unimodal sites ($n=35$) where antimode depth D_1 and secondary model depth D_2 is not available, we prescribe $D_1 = 70$ cm, $D_2 = 100$ cm that is consistent with the mean value from across all bimodal sites ($n=9$).

For root biomass and soil nutrient content that is only sampled once, we derive a single ϕ value per site. For soil moisture data however, we derive a time series of ϕ for soil moisture at each profile within each site. The use of time series (instead one time point) would allow us to examine the entire dynamics of soil moisture instead of just the mean or median, as the root status we observe (at a single time point) might be a response to a past short-period of soil moisture stress or incentive. For each time series, we visualize the full frequency distribution of soil moisture and subsequently calculate a list of distribution metrics: mean, median, max, min, standard deviation, coefficient of variance, 75th quantile, 25th quantile, interquartile range.

The depth resolution of our soil moisture data resolution (roughly, 6 cm, 16 cm, 26 cm, 56 cm, 86 cm, 116 cm, 146 cm, 176 cm) might not be ideal to distinguish D_1 and D_2 for certain sites. To compensate for this low depth resolution of soil moisture, we additionally examined the soil moisture dynamics of the surface sensor (6 cm) to evaluate whether the presence of bimodality is a result of surface drought.

Relative nutrient concentration

To calculate relative nutrient concentration in Fig. 4, we first transformed the original nutrient concentration (N, P, K, or Ca) by dividing them using the root biomass density (mg/cm^3) across all profiles of all 44 sites. For ease of cross-site comparison, we then rescaled the resulting relative nutrient concentration using relative nutrient concentration at surface depth. The rescaled relative nutrient concentration is thus dimensionless, and the surface soil has an average value 1.

Statistics

We used the neonUtilities R package⁸⁹ to access the following NEON data products: Root biomass and chemistry, Megapit (DP1.10066.001)⁹⁰ and Soil physical and chemical properties, Megapit (DP1.00096.001)⁹¹. All NEON datasets used in our analyses are summarized in Supplementary Table 2. We developed a classification model based random forest algorithm (Fig. 2a; R package randomForest). Given the unbalanced nature of our dataset (9 bimodal vs. 35 unimodal sites), we need to make sure that we predict the minority class (bimodal sites) equally well as the majority class (unimodal sites). The default behavior of random forest algorithms will prioritize the prediction accuracy of the majority class (thus maximizing overall accuracy). As a result, we modified the default voting rule such that the algorithm weighs more on the prediction accuracy of the minority class. We next searched the best performing model (highest bimodality prediction accuracy) by finding the best parameter combination across a grid of conditions (num.trees = 500, mtry = 6, min.node.size = 3, sample.fraction = 0.3, seed = 123). The best performing model after removing profile root biomass has the following parameter combination: num.trees = 500, mtry = 6, min.node.size = 3, sample.fraction =

0.3, seed = 123. The feature importance score shown in Fig. 2a is based on mean decrease in Gini coefficient, a measure of out-of-bag cross validated predictions. We sequentially dropped factors with the lowest Gini coefficient (such as temperature range, dry season precipitation, precipitation seasonality, etc.), when trimming the model would enhance the overall performance of the model. We used t-test to examine the feature differences between bimodal and unimodal sites (Fig. 2b, Supplementary Fig. 4). We first visualize the distribution of each feature splitted by modality and \log_{10} transforms the data to conform with normality. Then we used the F test to test equal variance between the unimodal and bimodal group to determine the use of Student's (equal variance) or Welch's t-test (unequal variance). We used the χ^2 test of independence to test the association between site modality and site vegetation cover (Fig. 2c). Due to the small sample size ($N=44$), we used the Pearson's Chi-squared test with simulated p -value (R base function `chisq.test`, `simulate.p.value = true`, 2000 replicates). We used linear regression to fit the relationship between rescaled relative nutrient abundance and depth (Fig. 4a, b). Rescaled relative nutrient abundance is \log_{10} transformed in all regression analyses, consistent with our visualization. All statistical analyses were performed using the R platform (R version 4.0.5).

Reporting summary

Further information on research design is available in the Nature Portfolio Reporting Summary linked to this article.

Data availability

All data is deposited at figshare (<https://doi.org/10.6084/m9.figshare.19525303>). Source data are provided with this paper.

Code availability

R scripts are deposited together with associated data on figshare (<https://doi.org/10.6084/m9.figshare.19525303>) and also available from the corresponding author upon request (mingzhen.lu@nyu.edu).

References

1. Norby, R. J. et al. Model-data synthesis for the next generation of forest free-air CO_2 enrichment (FACE) experiments. *N. Phytol.* **209**, 17–28 (2016).
2. Reich, P. B. et al. Nitrogen limitation constrains sustainability of ecosystem response to CO_2 . *Nature* **440**, 922–925 (2006).
3. Luo, Y. et al. Progressive nitrogen limitation of ecosystem responses to rising atmospheric carbon dioxide. *BioScience* **54**, 731 (2004).
4. Hedin, L. O. Biogeochemistry: signs of saturation in the tropical carbon sink. *Nature* **519**, 295–296 (2015).
5. Brienen, R. J. W. et al. Long-term decline of the Amazon carbon sink. *Nature* **519**, 344–348 (2015).
6. Hubau, W. et al. Asynchronous carbon sink saturation in African and Amazonian tropical forests. *Nature* **579**, 80–87 (2020).
7. Girardin, M. P. et al. No growth stimulation of Canada's boreal forest under half-century of combined warming and CO_2 fertilization. *Proc. Natl Acad. Sci. USA* **113**, E8406–E8414 (2016).
8. Eshel, A. & Beeckman, T. Plant Roots: The Hidden Half, *Fourth Edition*. (CRC Press, 2013).
9. Clemmensen, K. E. et al. Roots and associated fungi drive long-term carbon sequestration in boreal forest. *Science* **339**, 1615–1618 (2013).
10. McCormack, M. L. et al. Sensitivity of four ecological models to adjustments in fine root turnover rate. *Ecol. Modelling* **297**, 107–117 (2015).
11. Rasse, D. P., Rumpel, C. & Dignac, M.-F. Is soil carbon mostly root carbon? Mechanisms for a specific stabilisation. *Plant Soil* **269**, 341–356 (2005).
12. Sokol, N. W., Kuebbing, S. E., Karlsen-Ayala, E. & Bradford, M. A. Evidence for the primacy of living root inputs, not root or shoot litter, in forming soil organic carbon. *N. Phytol.* **221**, 233–246 (2019).

13. Cheng, W. et al. Synthesis and modeling perspectives of rhizosphere priming. *N. Phytol.* **201**, 31–44 (2014).

14. Malhotra, A. et al. Continental-scale relationships of fine root and soil carbon stocks hold in grasslands but not forests. *bioRxiv*, <https://doi.org/10.1101/2025.04.07.647629> (2025).

15. McCormack, M. L. et al. Redefining fine roots improves understanding of below-ground contributions to terrestrial biosphere processes. *N. Phytol.* **207**, 505–518 (2015).

16. Ma, Z. et al. Evolutionary history resolves global organization of root functional traits. *Nature* **555**, 94–97 (2018).

17. Kong, D. et al. Nonlinearity of root trait relationships and the root economics spectrum. *Nat. Commun.* **10**, 2203 (2019).

18. Lu, M. et al. Biome boundary maintained by intense belowground resource competition in world's thinnest-rooted plant community. *Proc. Natl Acad. Sci. USA* **119**, e2117514119 (2022).

19. Lu, M. & Hedin, L. O. Global plant–symbiont organization and emergence of biogeochemical cycles resolved by evolution-based trait modelling. *Nat. Ecol. Evol.* **3**, 239–250 (2019).

20. Bergmann, J. et al. The fungal collaboration gradient dominates the root economics space in plants. *Sci. Adv.* **6**, eaba3756 (2020).

21. Kattge, J. et al. TRY - a global database of plant traits. *Glob. Chang. Biol.* **17**, 2905–2935 (2011).

22. Guerrero-Ramírez, N. R. et al. Global root traits (GRoOT) database. *Glob. Ecol. Biogeogr.* **30**, 25–37 (2021).

23. Iversen, C. M. & McCormack, M. L. Filling gaps in our understanding of belowground plant traits across the world: an introduction to a Virtual Issue. *N. Phytol.* **231**, 2097–2103 (2021).

24. Tumber-Dávila, S. J., Schenk, H. J., Du, E. & Jackson, R. B. Plant sizes and shapes above and belowground and their interactions with climate. *N. Phytol.* **235**, 1032–1056 (2022).

25. Canadell, J. et al. Maximum rooting depth of vegetation types at the global scale. *Oecologia* **108**, 583–595 (1996).

26. Germon, A., Laclau, J.-P., Robin, A. & Jourdan, C. Tamm Review: Deep fine roots in forest ecosystems: Why dig deeper? *Forest Ecol. Manag.* **466**, 118135 (2020).

27. Pierret, A. et al. Understanding deep roots and their functions in ecosystems: an advocacy for more unconventional research. *Ann. Bot.* **118**, 621–635 (2016).

28. Maeght, J.-L., Rewald, B. & Pierret, A. How to study deep roots—and why it matters. *Front. Plant Sci.* **4**, 299 (2013).

29. Jackson, R. B., Moore, L. A., Hoffmann, W. A., Pockman, W. T. & Linder, C. R. Ecosystem rooting depth determined with caves and DNA. *Proc. Natl Acad. Sci. USA* **96**, 11387–11392 (1999).

30. Jackson, R. B., Sperry, J. S. & Dawson, T. E. Root water uptake and transport: using physiological processes in global predictions. *Trends Plant Sci.* **5**, 482–488 (2000).

31. McCulley, R. L., Jobbágy, E. G., Pockman, W. T. & Jackson, R. B. Nutrient uptake as a contributing explanation for deep rooting in arid and semi-arid ecosystems. *Oecologia* **141**, 620–628 (2004).

32. Balesdent, J. et al. Atmosphere–soil carbon transfer as a function of soil depth. *Nature* **559**, 599–602 (2018).

33. Schenk, H. J. & Jackson, R. B. The global biogeography of roots. *Ecological monographs* **72**, 311–328 (2002).

34. Kattge, J. et al. TRY plant trait database - enhanced coverage and open access. *Glob. Chang. Biol.* **26**, 119–188 (2020).

35. Keller, M., Schimel, D. S., Hargrove, W. W. & Hoffman, F. M. A continental strategy for the National Ecological Observatory Network. *Front. Ecol. Environ.* **6**, 282–284 (2008).

36. Kao, R. H. et al. NEON terrestrial field observations: designing continental-scale, standardized sampling. *Ecosphere* **3**, art115 (2012).

37. Gale, M. R. & Grigal, D. F. Vertical root distributions of northern tree species in relation to successional status. *Canadian J. Forest Res.* **17**, 829–834 (1987).

38. Jackson, R. B. et al. A global analysis of root distributions for terrestrial biomes. *Oecologia* **108**, 389–411 (1996).

39. Weber, N. A. Dimorphism in the African Oecophylla Worker Nd an Anomaly (Hym.: Formicidae). *Annal. Entomol. Soc. Am.* **39**, 7–10 (1946).

40. Zhang, C., Mapes, B. E. & Soden, B. J. Bimodality in tropical water vapour. *Quarterly J. Royal Meteor. Soc.* **129**, 2847–2866 (2003).

41. Balogh, M. L. et al. The bimodal galaxy color distribution: dependence on luminosity and environment. *Astrophys. J.* **615**, L101–L104 (2004).

42. Walter, H. Grasland, Savanne und Busch der arideren Teile Afrikas in ihrer ökologischen Bedingtheit. *Jahrb Wiss Bot.* **87**, 750–860 (1939).

43. Ward, D., Wiegand, K. & Getzin, S. Walter's two-layer hypothesis revisited: back to the roots!. *Oecologia* **172**, 617–630 (2013).

44. Houlton, B. Z., Morford, S. L. & Dahlgren, R. A. Convergent evidence for widespread rock nitrogen sources in Earth's surface environment. *Science* **360**, 58–62 (2018).

45. Porder, S., Vitousek, P. M., Chadwick, O. A., Chamberlain, C. P. & Hille, G. E. Uplift, Erosion, and Phosphorus Limitation in Terrestrial Ecosystems. *Ecosystems* **10**, 159–171 (2007).

46. Jobbágy, E. G. & Jackson, R. B. The distribution of soil nutrients with depth: Global patterns and the imprint of plants. *Biogeochemistry* **53**, 51–77 (2001).

47. Brady, N. C. & Weil, R. C. *The Nature and Properties of Soils*. (Prentice Hall, 2016).

48. Zhang, H. & Forde, B. G. Regulation of *Arabidopsis* root development by nitrate availability. *J. Exp. Bot.* **51**, 51–59 (2000).

49. Hodge, A. The plastic plant: root responses to heterogeneous supplies of nutrients. *New Phytologist* **162**, 9–24 (2004).

50. Iversen, C. M., Ledford, J. & Norby, R. J. CO₂ enrichment increases carbon and nitrogen input from fine roots in a deciduous forest. *N. Phytol.* **179**, 837–847 (2008).

51. Padilla, F. M. et al. Root plasticity maintains growth of temperate grassland species under pulsed water supply. *Plant Soil* **369**, 377–386 (2013).

52. Guntiñas, M. E., Leirós, M. C., Trasar-Cepeda, C. & Gil-Sotres, F. Effects of moisture and temperature on net soil nitrogen mineralization: A laboratory study. *Eur. J. Soil Biol.* **48**, 73–80 (2012).

53. Kulmatiski, A., Adler, P. B., Stark, J. M. & Tredennick, A. T. Water and nitrogen uptake are better associated with resource availability than root biomass. *Ecosphere* **8**, e01738 (2017).

54. LeBauer, D. S. & Treseder, K. K. Nitrogen limitation of net primary productivity in terrestrial ecosystems is globally distributed. *Ecology* **89**, 371–379 (2008).

55. Vitousek, P. M., Porder, S., Houlton, B. Z. & Chadwick, O. A. Terrestrial phosphorus limitation: mechanisms, implications, and nitrogen–phosphorus interactions. *Ecol. Appl.* **20**, 5–15 (2010).

56. Sardans, J. & Peñuelas, J. Potassium: a neglected nutrient in global change. *Global Ecol. Biogeogr.* **24**, 261–275 (2015).

57. Bond, W. J. Do nutrient-poor soils inhibit development of forests? A nutrient stock analysis. *Plant Soil* **334**, 47–60 (2010).

58. McLaughlin, S. B. & Wimmer, R. Calcium physiology and terrestrial ecosystem processes. *New Phytologist* **142**, 373–417 (1999).

59. Schenk, H. J. The shallowest possible water extraction profile: a null model for global root distributions. *Vadose Zone J.* **7**, 1119–1124 (2008).

60. Cardon, Z. G., Stark, J. M., Herron, P. M. & Rasmussen, J. A. Sagebrush carrying out hydraulic lift enhances surface soil nitrogen cycling and nitrogen uptake into inflorescences. *Proc. Natl Acad. Sci. USA* **110**, 18988–18993 (2013).

61. Miguez-Macho, G. & Fan, Y. Spatiotemporal origin of soil water taken up by vegetation. *Nature* **598**, 624–628 (2021).

62. Nippert, J. B. & Holdo, R. M. Challenging the maximum rooting depth paradigm in grasslands and savannas. *Funct. Ecol.* **29**, 739–745 (2015).

63. Nippert, J. B., Wieme, R. A., Ocheltree, T. W. & Craine, J. M. Root characteristics of C4 grasses limit reliance on deep soil water in tallgrass prairie. *Plant Soil* **355**, 385–394 (2012).

64. Iversen, C. M. Digging deeper: fine-root responses to rising atmospheric CO₂ concentration in forested ecosystems. *N. Phytol.* **186**, 346–357 (2010).

65. Tumber-Dávila, S. J. & Malhotra, A. Fast plants in deep water: introducing the whole-soil column perspective. *N. Phytol.* **225**, 7–9 (2020).

66. Bleby, T. M., McElrone, A. J. & Jackson, R. B. Water uptake and hydraulic redistribution across large woody root systems to 20 m depth. *Plant Cell Environ.* **33**, 2132–2148 (2010).

67. Jiang, P. et al. Linking reliance on deep soil water to resource economy strategies and abundance among coexisting understorey shrub species in subtropical pine plantations. *N. Phytol.* **225**, 222–233 (2020).

68. Bachofen, C. et al. Tree water uptake patterns across the globe. *N. Phytol.* **242**, 1891–1910 (2024).

69. Gherardi, L. A. & Sala, O. E. Global patterns and climatic controls of belowground net carbon fixation. *Proc. Natl Acad. Sci. USA* **117**, 20038–20043 (2020).

70. Pries, C. E. H. et al. Root litter decomposition slows with soil depth. *Soil Biol. Biochem.* **125**, 103–114 (2018).

71. Dungait, J. A. J., Hopkins, D. W., Gregory, A. S. & Whitmore, A. P. Soil organic matter turnover is governed by accessibility not recalcitrance. *Glob. Change Biol.* **18**, 1781–1796 (2012).

72. Schmidt, M. W. I. et al. Persistence of soil organic matter as an ecosystem property. *Nature* **478**, 49–56 (2011).

73. Rumpel, C. & Kögel-Knabner, I. Deep soil organic matter—a key but poorly understood component of terrestrial C cycle. *Plant Soil* **338**, 143–158 (2011).

74. Salome, C., Nunan, N., Pouteau, V., Lerch, T. Z. & Chenu, C. Carbon dynamics in topsoil and in subsoil may be controlled by different regulatory mechanisms. *Glob. Change Biol.* **16**, 416–426 (2010).

75. Bardgett, R. D. & van der Putten, W. H. Belowground biodiversity and ecosystem functioning. *Nature* **515**, 505–511 (2014).

76. Fontaine, S., Mariotti, A. & Abbadie, L. The priming effect of organic matter: a question of microbial competition? *Soil Biol. Biochem.* **35**, 837–843 (2003).

77. Dijkstra, F. A., Zhu, B. & Cheng, W. Root effects on soil organic carbon: a double-edged sword. *N. Phytol.* **230**, 60–65 (2021).

78. Zhu, B. et al. Rhizosphere priming effects on soil carbon and nitrogen mineralization. *Soil Biol. Biochem.* **76**, 183–192 (2014).

79. Kou, D. et al. Progressive nitrogen limitation across the Tibetan alpine permafrost region. *Nat. Commun.* **11**, 3331 (2020).

80. Malhotra, A. et al. Peatland warming strongly increases fine-root growth. *Proc. Natl Acad. Sci. USA* **117**, 17627–17634 (2020).

81. Nadelhoffer, K. J. & Raich, J. W. Fine root production estimates and belowground carbon allocation in forest ecosystems. *Ecology* **73**, 1139–1147 (1992).

82. Beaudette, D. E., Roudier, P. & O'Geen, A. T. Algorithms for quantitative pedology: A toolkit for soil scientists. *Comput. Geosci.* **52**, 258–268 (2013).

83. NEON (National Ecological Observatory Network). Soil water content and water salinity (DP1.00094.001). <https://doi.org/10.48443/ghry-qw46> (RELEASE-2022).

84. Ameijeiras-Alonso, J., Crujeiras, R. M. & Rodríguez-Casal, A. multi-mode: An R Package for Mode Assessment. *J. Stat. Softw.* **97**, 1–32 (2021).

85. Ameijeiras-Alonso, J., Crujeiras, R. M. & Rodríguez-Casal, A. Mode testing, critical bandwidth and excess mass. *TEST* **28**, 900–919 (2019).

86. Fick, S. E. & Hijmans, R. J. WorldClim 2: new 1-km spatial resolution climate surfaces for global land areas. *Int. J. Climatol.* **37**, 4302–4315 (2017).

87. Trabucco, A. & Zomer, R. J. Global Aridity Index (Global-Aridity) and Global Potential Evapo-Transpiration (Global-PET) Geospatial Database. (2009).

88. Zhang, Y. et al. A global moderate resolution dataset of gross primary production of vegetation for 2000–2016. *Sci. Data* **4**, 170165 (2017).

89. Lunch, C. K., Laney, C. M. & NEON (National Ecological Observatory Network). *neonUtilities: Utilities for Working with NEON Data*. (2020).

90. NEON (National Ecological Observatory Network). Root biomass and chemistry, Megapit (DP1.10066.001). <https://doi.org/10.48443/xmbe-7b55> (RELEASE-2022).

91. NEON (National Ecological Observatory Network). Soil physical and chemical properties, Megapit (DP1.00096.001). <https://doi.org/10.48443/10dn-8031> (RELEASE-2022).

Acknowledgements

This work was supported by the Santa Fe Institute Omidyar Fellowship to M.L. We thank resident faculty members and postdocs at the Santa Fe Institute and members of the Jackson lab for helpful comments on the manuscript. The National Ecological Observatory Network (NEON) is a program sponsored by the U.S. National Science Foundation and operated under cooperative agreement by Battelle. This material is based in part upon work supported by the U.S. National Science Foundation through the NEON Program. A.M. was supported by the Swiss National Science Foundation (project 200021_215214) and COMPASS-FME, a multi-institutional project supported by the U.S. Department of Energy, Office of Science, Biological and Environmental Research as part of the Environmental System Science Program. The Pacific Northwest National Laboratory is operated for DOE by Battelle Memorial Institute under contract DE-AC05-76RL01830. S.J.T.D. was supported by the Harvard Forest LTER Postdoctoral Fellowship and the NSF Funded LTER Program (NSF-DEB-LTER 1832210).

Author contributions

M.L. and S.W. conceived and designed research, M.L. performed analyses with input from S.W., R.B.J., A.M., and S.J.T.D., M.L. drafted the paper and S.W., A.M., S.J.T.D., S.W-L, M.L.M., X.W., and R.B.J. contributed significantly to writing and editing.

Competing interests

The authors declare no competing interests.

Additional information

Supplementary information The online version contains supplementary material available at <https://doi.org/10.1038/s41467-025-60055-2>.

Correspondence and requests for materials should be addressed to Mingzhen Lu.

Peer review information *Nature Communications* thanks Dietrich Hertel and the other, anonymous, reviewer(s) for their contribution to the peer review of this work. A peer review file is available.

Reprints and permissions information is available at <http://www.nature.com/reprints>

Publisher's note Springer Nature remains neutral with regard to jurisdictional claims in published maps and institutional affiliations.

Open Access This article is licensed under a Creative Commons Attribution-NonCommercial-NoDerivatives 4.0 International License, which permits any non-commercial use, sharing, distribution and reproduction in any medium or format, as long as you give appropriate credit to the original author(s) and the source, provide a link to the Creative Commons licence, and indicate if you modified the licensed material. You do not have permission under this licence to share adapted material derived from this article or parts of it. The images or other third party material in this article are included in the article's Creative Commons licence, unless indicated otherwise in a credit line to the material. If material is not included in the article's Creative Commons licence and your intended use is not permitted by statutory regulation or exceeds the permitted use, you will need to obtain permission directly from the copyright holder. To view a copy of this licence, visit <http://creativecommons.org/licenses/by-nc-nd/4.0/>.

© The Author(s) 2025